

## Supplemental material

Silver et al., <https://doi.org/10.1083/jcb.201807106>

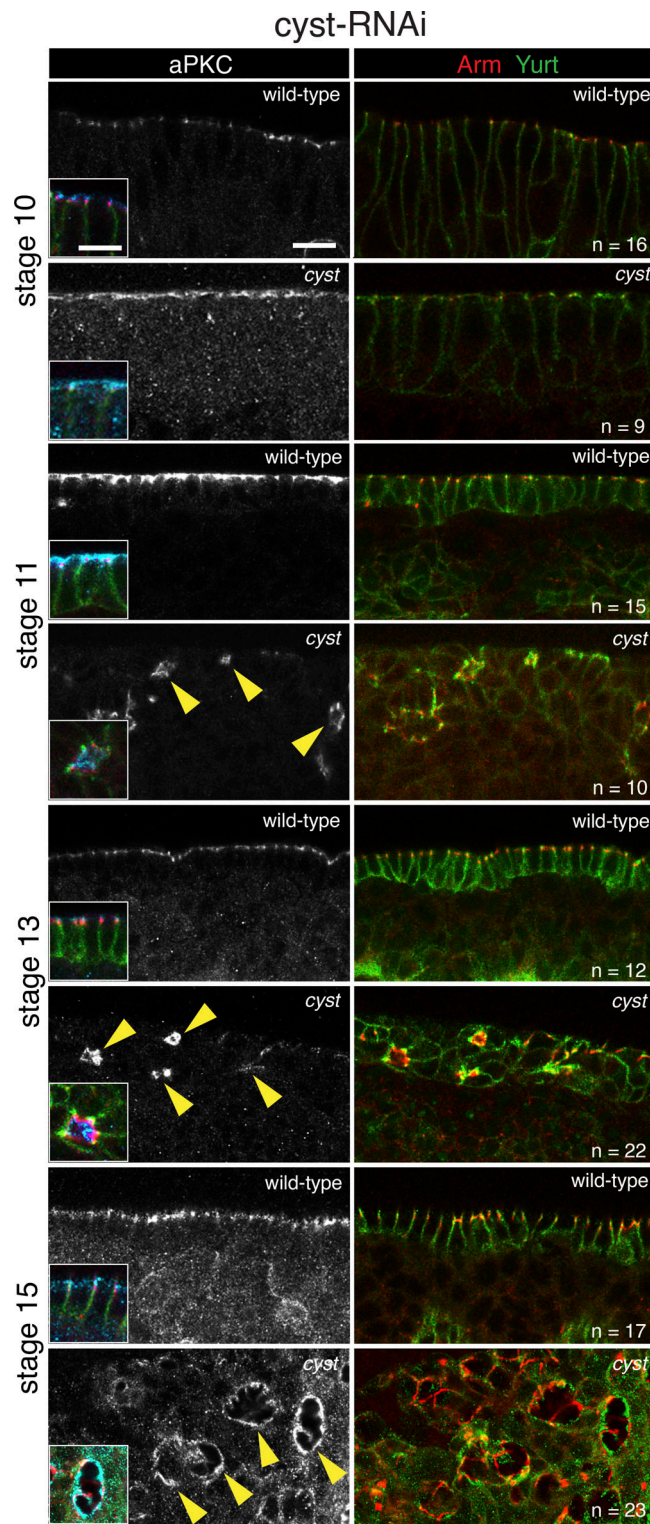


Figure S1. **aPKC distribution in *cyst* RNAi embryos.** Staining of *cyst* RNAi embryos compared with wild-type controls for the apical marker aPKC, the junctional marker Arm, and the basolateral marker Yrt. All panels show side views of the ectoderm or epidermis at the indicated stages. Epithelial cysts in *cyst*-compromised embryos are evident in stage-11, -13 and -15 embryos (arrowheads) but not at stage 10. Markers show normal subcellular distributions with apical markers in epithelial cysts facing the lumen where cuticle will be secreted (see Fig. 1, C–E). Insets show triple-labeled cells with aPKC shown in blue. Scale bars, 10  $\mu$ m; insets, 5  $\mu$ m.

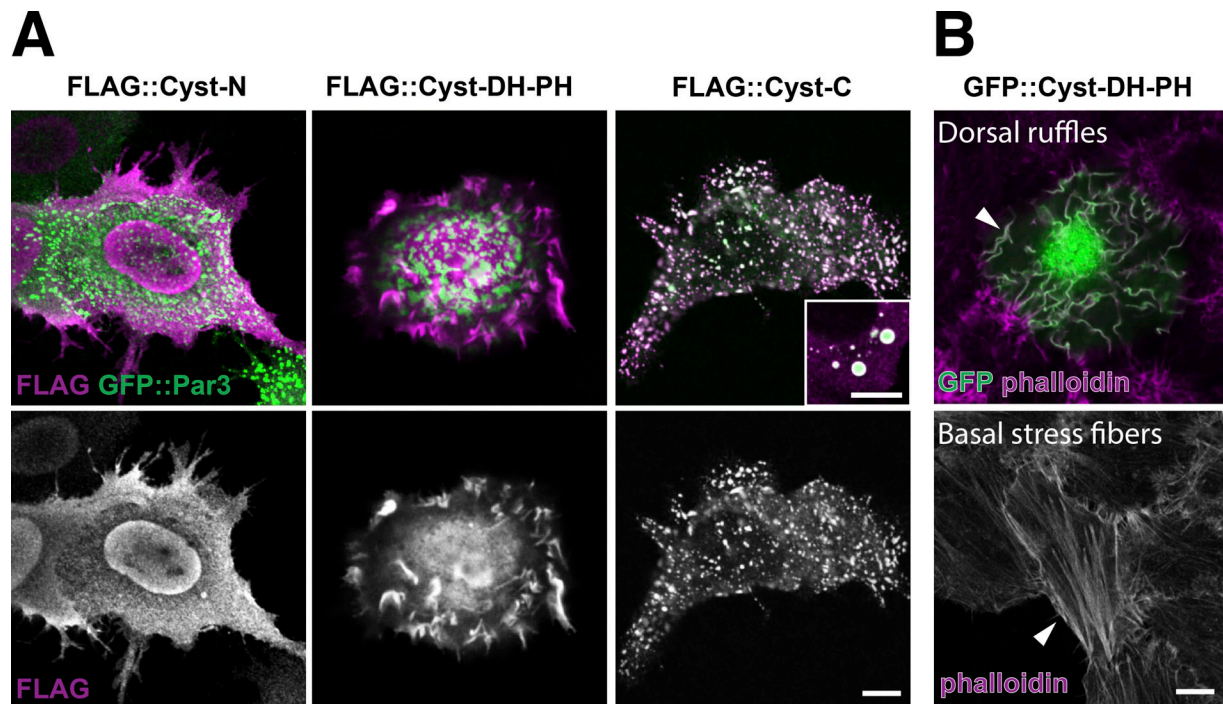
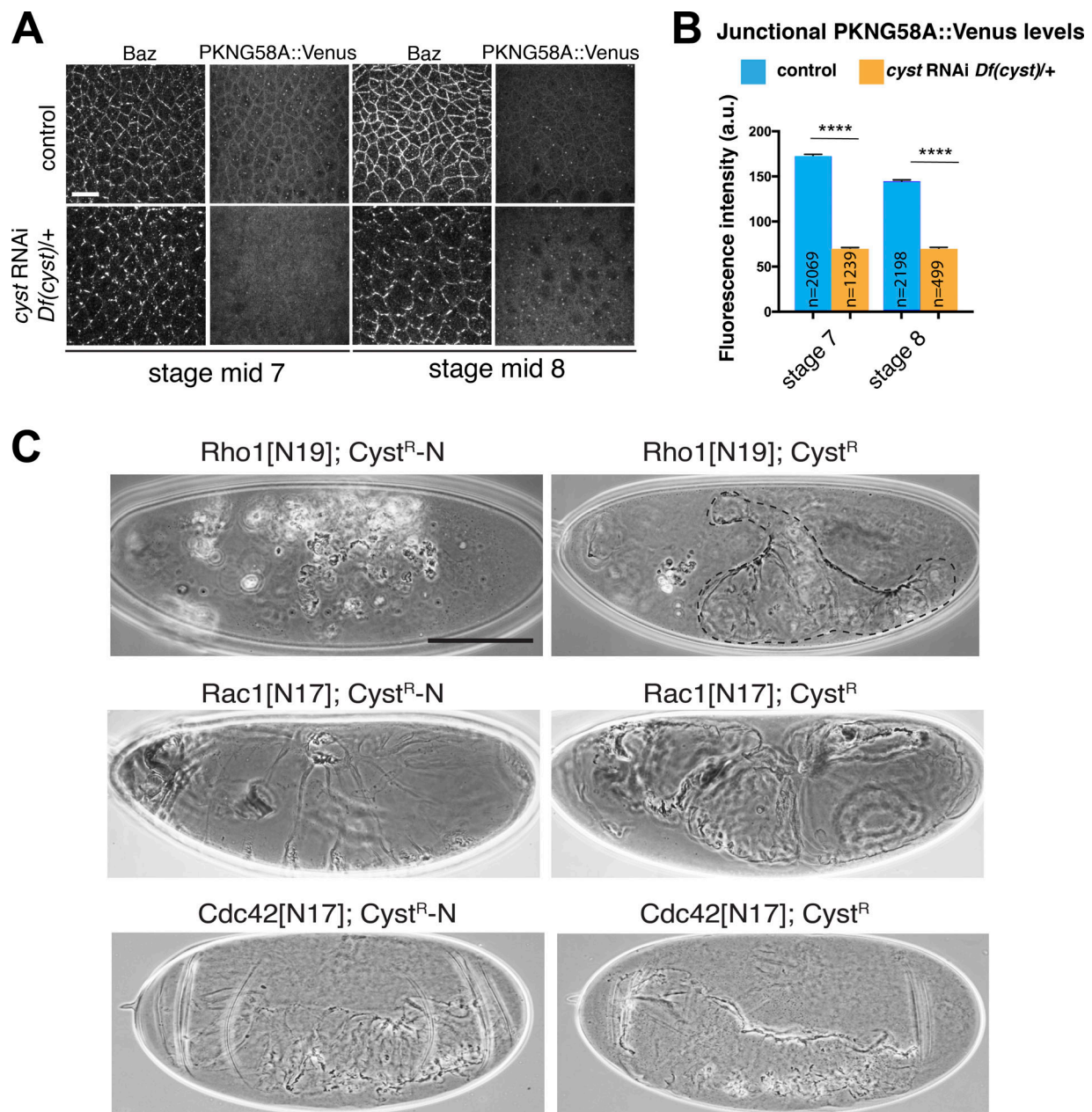


Figure S2. **Cyst coaggregates with Par3 and elicits formation of ruffles and stress fibers.** **(A)** Immunostainings of HeLa cells coexpressing various FLAG-tagged Cyst fragments and GFP::Par3. FLAG::Cyst-N and FLAG::Cyst-DH-PH did not colocalize with GFP::Par3 ( $n > 100$ ), whereas colocalization in cytoplasmic puncta (close-up shown in inset) was observed between FLAG::Cyst-C and GFP::Par3 ( $n > 100$ ). Scale bars, 5  $\mu\text{m}$ . **(B)** Immunostainings of HeLa cells expressing GFP::Cyst-DH-PH with indicated markers. Dorsal and basal views are shown. Arrowheads indicate dorsal ruffles (top panel) or stress fiber (bottom panel). Approximately 20% of cells displayed dorsal ruffles or stress fibers ( $n > 100$ ). Scale bar, 5  $\mu\text{m}$ .



**Figure S3. Cyst interacts with Rho1.** (A) Junctional levels of active Rho1 detected with PKNG58A::Venus biosensor at stages 7 and 8 in control and *Cyst*-depleted embryos. Baz labels Ajs. Notice a decrease in the levels of active Rho1 at cell-cell junctions and junctional fragmentation in *Cyst*-depleted embryos. This Rho1 sensor also labels centrosomes (cytoplasmic bright dots), a signal that is maintained in *Cyst*-depleted embryos and controls and serves as internal control labeling. Scale bar, 10  $\mu$ m. (B) Quantification of junctional PKNG58A::Venus levels at stages 7 and 8 in control and *Cyst*-depleted embryos. Controls: 13 embryos at stage 7 and 12 embryos at stage 8; *Cyst*-depleted: 9 embryos at stage 7 and 4 embryos at stage 8; *n* values indicate number of cell edges analyzed. \*\*\*\*,  $P = 2.4 \times 10^{-207}$  (left) and  $P = 1.8 \times 10^{-86}$  (right; Kolmogorov-Smirnov test). Data presented as mean + SEM. (C) Cuticles are shown for the indicated genotypes. Coexpression of *Cyst*<sup>R</sup> with DN mutant Rho1[N19] using *mat*-Gal4 partially rescues the Rho1[N19] phenotype from cuticle vesicles to a cuticle shield (dashed line). As a control, we coexpressed of Rho1[N19] with *Cyst*<sup>R-N</sup>, which is a nonfunctional *Cyst* protein (see Fig. 6). Rho1[N19] *Cyst*<sup>R-N</sup>: Among 55 embryos examined, 54 had cuticle vesicles only and 1 had a cuticle shield. Rho1[N19] *Cyst*<sup>R</sup>: Among 60 embryos examined, 3 had cuticle vesicles only and 57 had cuticle shields or more intact cuticles. *Cyst*<sup>R</sup> coexpression with a DN Rac1[N17] using *da*-Gal4 did not ameliorate the Rac1[N17] phenotype ( $n = 42$ ) compared with Rac1[N17] *Cyst*<sup>R-N</sup> control ( $n = 28$ ). *Cyst*<sup>R</sup> coexpression with DN Cdc42[N17] using *da*-Gal4 did not change the DN-Cdc42 phenotype ( $n = 31$ ) compared with Cdc42[N17] *Cyst*<sup>R-N</sup> control ( $n = 29$ ). Scale bar, 100  $\mu$ m.

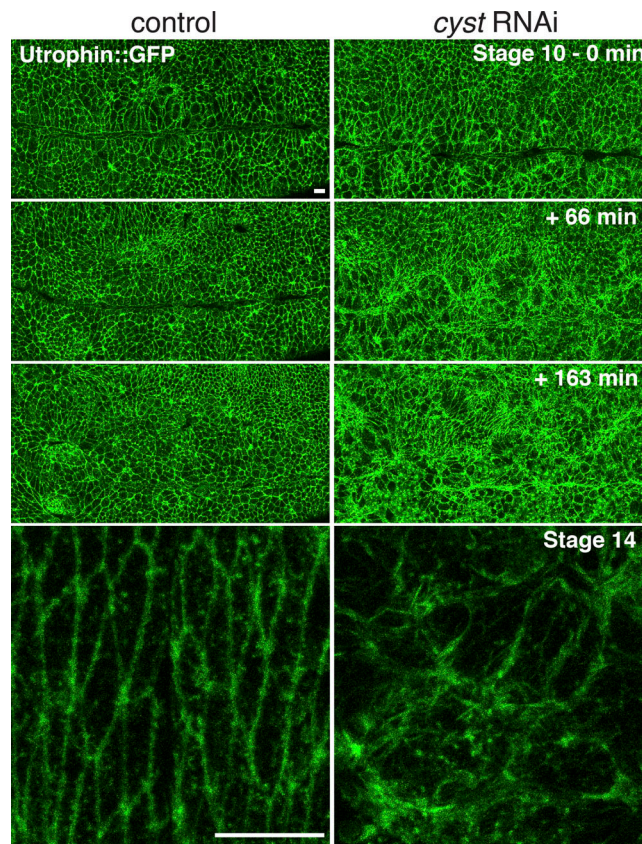
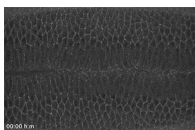
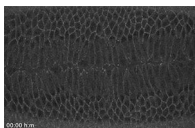


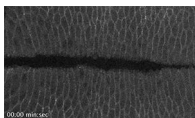
Figure S4. **Cyst regulates actin dynamics.** Z-projections taken from live embryos expressing Utrophin::GFP in a control ( $n = 5$ ) or *cyst* shRNA ( $n = 5$ ) background. The ventral ectoderm is shown. The loss of Cyst leads to aberrant Utrophin::GFP dynamics with an increase in Utrophin::GFP levels throughout the ectoderm. Scale bar, 10  $\mu\text{m}$ . Corresponds to Videos 9 and 10.



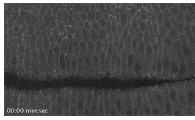
Video 1. **DEcad::GFP in control embryo.** Live imaging of a control embryo expressing DEcad::GFP under the control of the endogenous promoter. Anterior is left and ventral is down. See Fig. 2 for stills and description. Display rate, 15 frames/s.



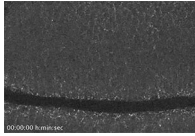
Video 2. **DEcad::GFP in cyst RNAi embryo.** Live imaging of a *cyst* RNAi embryo expressing DEcad::GFP under the control of the endogenous promoter. Anterior is left and ventral is down. See Fig. 2 for stills and description. Display rate, 15 frames/s.



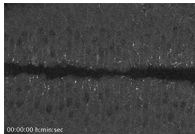
Video 3. **AnillinRBD::GFP biosensor expression in a control embryo.** Note accumulation of this biosensor at the AJs in the ectoderm, as well as at the cytokinetic furrows and midbodies during cell divisions. Images were acquired with 15-s intervals between stages 7 and 9 (3–3:50 h after egg laying). Anterior is left and ventral is down. See Fig. 8 A for stills and further description. Display rate, 20 frames/s.



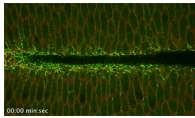
Video 4. **AnillinRBD::GFP biosensor expression in a cyst RNAi embryo.** The junctional pool of AnillinRBD::GFP is strongly reduced compared with control embryos (Video 3). The probe still accumulates at the cytokinetic furrow and midbodies during and after cell division, similarly to control embryos. Images were acquired with 15-s intervals between stages 7 and 9 (3–3:50 h after egg laying). Anterior is left and ventral is down. See Fig. 8 A for stills and further description. Display rate, 20 frames/s.



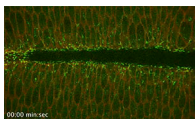
Video 5. **Myosin II dynamics in a mock-RNAi control embryo.** Embryo expressing shRNA against mCherry (mock-RNAi) and myosin II::GFP. Note two populations of myosin II, one associated with the AJs and another dynamic, pulsatile pool at the medial-apical cell cortex. Images were acquired with 15-s intervals between stages 7 and 10 (3–4:49 h after egg laying). Anterior is left and ventral is down. See Fig. 9 B for stills and further description. Display rate, 15 frames/s.



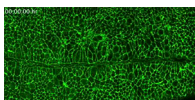
Video 6. **Myosin II dynamics in a cyst RNAi embryo.** Embryo maternally depleted for *cyst* (mothers: *Df(cyst)/+* *cyst* RNAi) expressing myosin II::GFP. Note a decrease in junctional and medial-apical levels of myosin II compared with control (Video 5). Images were acquired with 15-s intervals between stages 7 and 10 (3–4:49 h after egg laying). Anterior is left and ventral is down. See Fig. 9 B for stills and further description. Display rate, 15 frames/s.



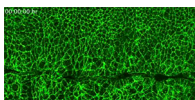
Video 7. **Myosin II dynamics in a control embryo.** Wild-type embryo expressing Myosin II::GFP (green) and the membrane marker GAP43::mCherry (red). Note two populations of myosin II: one associated with the cell junctions and another dynamic, pulsatile pool at the medial-apical cell cortex. Images were acquired with 15-s intervals between stages 7 and 9 (3–3:58 h after egg laying). Anterior is left and ventral is down. See Fig. 9 C for stills and further description. Display rate, 15 frames/s.



Video 8. **Myosin II dynamics in a *crb* RNAi embryo.** *crb* RNAi embryo expressing myosin II::GFP (green) and the membrane marker GAP43::mCherry (red). Note a decrease in the junctional levels of myosin II and an increase in medial-apical myosin II levels. Images were acquired with 15-s intervals between stages 7 and 9 (3–3:58 h after egg laying). Anterior is left and ventral is down. See Fig. 9 C for stills and further description. Display rate, 15 frames/s.



Video 9. **Actin dynamics in control embryo.** Live imaging of a control embryo expressing Utrophin::GFP. The ventral ectoderm is followed from stage 10 + 1:30 h at a time resolution of 30 s. See Fig. S4 for stills and description. Display rate, 21 frames/s.



Video 10. **Actin dynamics in a cyst RNAi embryo.** Live imaging of a cyst RNAi embryo expressing Utrophin::GFP. The ventral ectoderm is followed from stage 10 + 1:30 h at a time resolution of 30 s. See Fig. S4 for stills and description. Display rate, 21 frames/s.